

High-precision direct decay energy measurements of the electron-capture decay of ^{97}Tc

Zhuang Ge,^{1,*} Tommi Eronen,^{1,†} Vasile Alin Sevestean,^{2,3,4,‡} Marlom Ramalho,¹ Ovidiu Nițescu,^{2,4} Stefan Ghinescu,^{2,3,4} Sabin Stoica,² Jouni Suhonen,^{1,2,§} Antoine de Roubin,^{5,6,¶} Dmitrii Nesterenko,¹ Anu Kankainen,¹ Pauline Ascher,⁶ Samuel Ayet San Andres,⁷ Olga Beliuskina,¹ Pierre Delahaye,⁸ Mathieu Flayol,⁶ Mathias Gerbaux,⁶ Stéphane Grévy,⁶ Marjut Hukkanen,^{1,9} Arthur Jaries,¹ Ari Jokinen,¹ Audric Husson,⁶ Daid Kahl,^{10,**} Joel Kostensalo,¹¹ Jenni Kotila,^{12,13} Iain Moore,¹ Stylianos Nikas,¹ Jouni Ruotsalainen,¹ Marek Stryczyk,¹ and Ville Virtanen¹

¹*Department of Physics, University of Jyväskylä, P.O. Box 35, FI-40014, Jyväskylä, Finland*

²*International Centre for Advanced Training and Research in Physics,
P.O. Box MG12, 077125 Bucharest-Măgurele, Romania*

³*Faculty of Physics, University of Bucharest, 405 Atomîștilor,
P.O. Box MG11, 077125 Bucharest-Măgurele, Romania*

⁴*“Horia Hulubei” National Institute of Physics and Nuclear Engineering,
30 Reactorului, POB MG-6, RO-077125 Bucharest-Măgurele, Romania*

⁵*KU Leuven, Instituut voor Kern- en Stralingsfysica, B-3001 Leuven, Belgium*

⁶*Université de Bordeaux, CNRS/IN2P3, LP2I Bordeaux, UMR 5797, F-33170 Gradignan, France*

⁷*Instituto de Fisica Corpuscular, CSIC-UV, 46980, Gradignan, Spain*

⁸*GANIL, CEA/DSM-CNRS/IN2P3, Bd Henri Becquerel, 14000 Caen, France*

⁹*Centre d’Etudes Nucléaires de Bordeaux Gradignan, UMR 5797 CNRS/IN2P3 - Université de Bordeaux,
19 Chemin du Solarium, CS 10120, F-33175 Gradignan Cedex, France*

¹⁰*Extreme Light Infrastructure - Nuclear Physics, Horia Hulubei National Institute for
R&D in Physics and Nuclear Engineering (IFIN-HH), Bucharest-Magurele 077125, Romania*

¹¹*Natural Resources Institute Finland, Yliopistokatu 6B, FI-80100, Joensuu, Finland*

¹²*Finnish Institute for Educational Research, University of Jyväskylä, P.O. Box 35, FI-40014, Jyväskylä, Finland*

¹³*Center for Theoretical Physics, Sloane Physics Laboratory Yale University, New Haven, Connecticut 06520-8120, USA*
(Dated: February 10, 2025)

A direct measurement of the ground-state-to-ground-state electron-capture decay Q (Q_{EC}) value of ^{97}Tc has been conducted employing the high resolving power phase-imaging ion-cyclotron-resonance technique with the double Penning trap mass spectrometer JYFLTRAP. The resulting Q_{EC} value for ^{97}Tc is 324.82(21) keV, exhibiting a precision approximately 19 times higher than the value adopted in the newest Atomic Mass Evaluation (AME2020) and differing by 1.2σ . Furthermore, by combining this refined Q value with nuclear energy-level data for the decay-daughter ^{97}Mo , a potential ultra-low Q -value transition, possibly of allowed type, ^{97}Tc ($9/2^+$, ground state) \rightarrow $^{97}\text{Mo}^*$ (320(1) keV), was evaluated for future long-term neutrino-mass determination experiments. The ground-state-to-excited-state electron-capture decay Q value (Q_{EC}^*) of this transition was determined to be 4.8(10) keV, confirming it to be energetically allowed with a confidence level of exceeding 4σ . The captures of electrons occupying the L and higher shells for this transition are energetically allowed, giving a value of 2.0(10) keV for the closest distance of Q_{EC}^* to the allowed binding energy of the L1 shell. To predict partial half-lives and energy-release distributions for this transition, the atomic self-consistent many-electron Dirac–Hartree–Fock–Slater method and the nuclear shell model have been employed. Dominant correction terms such as exchange and overlap corrections, as well as shake-up and shake-off effects, were included in the final results. Moreover, the normalized distribution of released energy in the electron-capture decay of ^{97}Tc to excited states of ^{97}Mo , is compared with that of ^{163}Ho , which is being used for electron-neutrino-mass determination. A pseudo-experiment technique was introduced to calculate error propagation in half-life and the 68% confidence interval for normalized energy distributions.

I. INTRODUCTION

Neutrinos are electrically neutral fermions that interact only via the weak force and gravity, and they have an incredibly tiny rest mass compared to other elementary particles. Neu-

trinos do not participate in electromagnetic or strong interactions, thus allowing them to pass through matter unimpeded. Up to now, three neutrino flavors have been found: electron neutrino (ν_e), muon neutrino (ν_μ), and tau neutrino (ν_τ). For each neutrino, there also exists a corresponding antineutrino, which also has spin of 1/2 and no electric charge [1]. Although neutrinos were initially thought to be massless as estimated by the standard model (SM), the three neutrino mass eigenstates do not show a one-to-one correspondence to the three flavors, each flavor being a quantum superposition of all three mass states [2]. Neutrinos oscillate between flavors, making their detection even more intriguing [3–5]. Neutrino-oscillation experiments reveal that at least two neutrino-mass eigenstates have a non-zero rest mass, leading to a mass difference be-

* Corresponding author; zhuang.z.ge@jyu.fi

† Corresponding author; tommi.eronen@jyu.fi

‡ Corresponding author; sevestean.alin@theory.nipne.ro

§ Corresponding author; jouni.t.suhonen@jyu.fi

¶ Present address: Université de Caen Normandie, CNRS/IN2P3, LPC Caen UMR6534, F-14000 Caen, France

** Present address: Facility for Rare Isotope Beams, Michigan State University, 640 South Shaw Lane East Lansing, MI 48824, USA

tween the three mass eigenstates. Laboratory experiments and cosmological observations have provided experimental data on differences in the squares of the neutrino masses, an upper limit on their sum, and an upper limit on the mass of the electron (anti)neutrino. Among these experiments, the most direct and model-independent way to pin down the exact mass value of the electron antineutrino ($m_{\bar{\nu}_e}$) is to measure the electron energy spectrum of single β^- decay, e.g., the Karlsruhe Tritium Neutrino (KATRIN) experiment [6–8], which has recently pushed the absolute electron antineutrino mass scale boundary to $0.45 \text{ eV}/c^2$ at the 90% confidence level (CL) [9]. KATRIN will finally set the $m_{\bar{\nu}_e}$ upper limit with a sensitivity of $0.2 \text{ eV}/c^2$ at 90% CL. Other single- β^- -decay experiments, Project 8 and PTOLEMY project, using cyclotron radiation emission spectroscopy and the development of atomic tritium sources, will eventually allow a sensitivity of tritium-based neutrino-mass experiments to $m_{\bar{\nu}_e}$ beyond the design sensitivity of KATRIN [10, 11] down to $0.04 \text{ eV}/c^2$. An alternative method, employing electron capture in ^{163}Ho (ECHO), an experiment to calorimetrically measure the electron-capture (EC) deexcitation spectrum [12–14], has set a current limit of $150 \text{ eV}/c^2$ for the electron neutrino mass [14].

In single- β^- -decay experiments aimed at determining the mass of the electron antineutrino, a Q value of the decay as small as possible is sought. A smaller Q value leads to a higher fraction of effective decays within a given energy interval ΔE near the endpoint region. Currently, the running direct (anti)neutrino-mass-determination experiments rely exclusively on ground-state-to-ground-state (gs-to-gs) decay cases, such as ^3H (β^- decay) and ^{163}Ho (EC). However, ongoing intensive searches are actively exploring isotopes having low Q -value ground-state-to-excited-state (gs-to-es) β^-/EC decays [15–17] using high-precision Penning-trap mass spectrometry (PTMS) including JYFLTRAP, LEBIT, CPT, ISOTRAP, and SHIPTRAP Penning traps [18–32]. PTMS is the most precise and accurate technique for determining atomic masses and Q values. It remains the only direct method capable of measuring decay Q values to sub-keV precision or better, allowing verification of potential ultra-low ($< 1 \text{ keV}$) Q -value transitions.

For the nuclide ^{97}Tc , there exists a potential low Q -value gs-to-es EC transition, ^{97}Tc ($9/2^+$, ground state) \rightarrow $^{97}\text{Mo}^*$ ($320(1) \text{ keV}$ [33], excited state), that could be employed for neutrino-mass detection. This speculated allowed transition, having a gs-to-es Q -value of $0.0(41) \text{ keV}$ deduced from the existing experimental data [33, 34], makes itself a candidate for an ultra-low Q -value transition. However, the Q value of the decay to the excited state in the daughter nucleus is known with only 4.1 keV precision. This uncertainty arises from the combined uncertainties in the gs-to-gs EC Q value (4 keV) adopted from [34] and in the excitation energy (1 keV) from [33]. As a result, a definitive conclusion regarding its energetic feasibility cannot be drawn solely from the current experimental information. To further determine whether this specific decay is energetically feasible and whether it falls into the ultra-low category, experimental measurements of the gs-to-gs decay Q value and the excitation energy of the state in the daughter nucleus are required.

Here, we present the first direct measurement of the gs-to-gs EC Q value for ^{97}Tc using the JYFLTRAP Penning-trap mass spectrometer. The precise Q value obtained, along with current nuclear energy-level information for excited states of ^{97}Tc , is employed to refine the gs-to-es Q values. The possible ultra-low Q -value transition in ^{97}Tc is verified with the newly determined experimental data. We confirm the transition to be energetically allowed. To explore the viability of this transition for neutrino-mass detection, we utilize two computational methods: the atomic self-consistent many-electron Dirac–Hartree–Fock–Slater method and the nuclear shell model. These approaches enable us to predict the partial half-lives and energy-release distributions for the relevant EC-decay transition.

II. EXPERIMENTAL METHOD

The experiment was carried out at the Ion Guide Isotope Separator On-Line facility (IGISOL) at the University of Jyväskylä, Finland [35, 36]. Figure 1 gives a schematic view of the experimental setup.

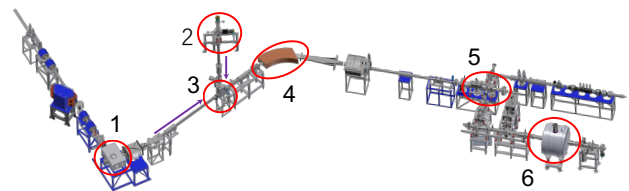


FIG. 1. (Color online). Schematic view of the IGISOL facility. The $^{97}\text{Tc}^+$ ions were generated via proton-induced fusion-evaporation reactions on a natural Mo target in the IGISOL target chamber (1). Simultaneously, stable $^{97}\text{Mo}^+$ ions were created at the offline ion source station (2) using glow discharge. An electrostatic kicker (3) was utilized for ion-beam selection. A dipole magnet (4) selected singly-charged ions with the same mass number. The RFQ-CB (5) was employed for ion cooling and bunching, and the final Q -value and mass measurements were performed with the JYFLTRAP Penning-trap setup (6).

^{97}Tc ions were generated in fusion-evaporation reactions between a natural molybdenum target foil irradiated with a few μA of a proton beam of energy 45 MeV produced by the K-130 cyclotron. The secondary ions were stopped in a small volume gas cell filled with helium at a pressure of around 100 mbar as shown in Fig. 1. There, the ions end up mainly singly charged from charge-exchange reactions. The predominantly singly charged ions are extracted from the gas cell by helium gas flow and are guided with electric fields facilitated by differential pumping and a sextupole ion guide (SPIG) [37]. Subsequently, the ions were accelerated using a 30 kV electric potential and transported to the 55° dipole magnet for isobaric mass separation with a typical mass resolving power of approximately 500. The isobarically separated ions with mass-to-charge ratio $A/q = 97$ (including reaction products such as $^{97}\text{Nb}^+$, $^{97m}\text{Tc}^+$, $^{97}\text{Tc}^+$, and $^{97}\text{Mo}^+$) were then directed to a radiofrequency-quadrupole cooler-buncher

(RFQ-CB) [38], where they underwent accumulation, cooling, and bunching. To produce the decay-daughter ion $^{97}\text{Mo}^+$ samples, an offline glow-discharge ion source was used [39]. Additionally, a 90° electrostatic bender, as presented in Fig. 1, selectively guided ions either from the online target station or the offline ion source for downstream transmission to the RFQ-CB.

The cooled and bunched ions from the RFQ-CB, were further directed to the JYFLTRAP [40], which consists of two cylindrical Penning traps within a 7-T superconducting solenoid, for the final mass and Q -value measurements. The first trap, filled with helium buffer gas, serves as a purification trap and is employed for isobaric purification using the sideband buffer gas cooling technique [41] with a resolving power of approximately 10^5 . To select the $^{97}\text{Tc}^+$ ion samples, this method could separate the aforementioned ions of $^{97}\text{Nb}^+$, but lacked sufficient mass resolving power to eliminate $^{97}\text{Mo}^+$ and $^{97m}\text{Tc}^+$ ions.

Mono-isotopic samples of $^{97}\text{Tc}^+$ were therefore prepared using the coupling of the dipolar excitation with Ramsey's method of time-separated oscillatory fields [42] and the phase-imaging ion-cyclotron-resonance (PI-ICR) technique [43, 44], as described in [29]. A Ramsey-type dipole excitation frequency scan in the second trap, employing a 2 ms (On) - 98 ms (Off) - 2 ms (On) excitation pattern, was used. The ions of interest were selectively chosen by filtering through positional gates using PI-ICR identification with a 436 ms phase accumulation time.

The PI-ICR method [43, 44] is used to measure the Q value via the actual measurements of the cyclotron frequency,

$$v_c = \frac{1}{2\pi} \frac{q}{m} B, \quad (1)$$

where m is the mass of the ion, q the charge and B the magnetic field of the trap. The PI-ICR technique is around 25 times faster than the conventional time-of-flight ion-cyclotron-resonance (TOF-ICR) method used to achieve the same precision with a similar experimental condition [43–46]. The scheme of the PI-ICR technique used at JYFLTRAP [44] relies on the direct measurements of the magnetron motion and the reduced cyclotron motion at the same time while projecting the radial ion motion onto a position-sensitive MCP detector. The angle α_c between the two phase images of the projected radial motions, obtained from two timing patterns for determining the cyclotron frequency v_c , is defined with respect to the center spot: $\alpha_c = \alpha_+ - \alpha_-$. Specifically, α_+ and α_- correspond to the polar angles of the magnetron and reduced cyclotron motion phases. The cyclotron frequency v_c is determined from the α_c measurements during the phase accumulation time t_{acc} :

$$v_c = \frac{\alpha_c + 2\pi n_c}{2\pi t_{acc}}, \quad (2)$$

where n_c represents the full number of revolutions of the measured ions. To unambiguously assign n_c in Eq. (2), different accumulation times were used for $^{97}\text{Tc}^+$. The actual measurements employed an accumulation time of 436 ms to determine the final cyclotron frequency v_c for both $^{97}\text{Tc}^+$ and $^{97}\text{Mo}^+$

ions, ensuring that any leaked isobaric contaminant would not overlap with the ions of interest.

To minimize any shifts in the v_c ratio of the $^{97}\text{Tc}^+ - ^{97}\text{Mo}^+$ pair, the positions of the phase spots for the magnetron and reduced cyclotron motions were carefully chosen to maintain the angle α_c within a few degrees. This was done to account for the conversion of the reduced cyclotron motion to the magnetron motion and the potential distortion of the ion-motion projection onto the detector, ensuring that the shift remained well below 10^{-10} [45]. Figure 2 shows a representative measurement with "reduced cyclotron" and "magnetron" phase spots relative to the center spot. During the measurements, the excitation delay of v_+ was systematically scanned over one magnetron period, while the extraction delay varied over one cyclotron period, accounting for any residual motion that might have affected the spots. The interleaved measurements of v_c for $^{97}\text{Tc}^+ - ^{97}\text{Mo}^+$ ions had a total data accumulation time of approximately 4.9 hours.

The gs-to-gs EC Q value (Q_{EC}), the mass difference of the decay pair, can be derived from their measured cyclotron frequency ratio $R (= \frac{v_{c,d}}{v_{c,p}})$:

$$Q_{EC} = (M_p - M_d)c^2 = (R - 1)(M_d - qm_e)c^2 + (R \cdot B_d - B_p), \quad (3)$$

where M_p and M_d are the masses of the parent and daughter atoms, and m_e the mass of an electron. The electron binding energies of the parent and daughter atoms, denoted as B_p and B_d , are neglected due to their small values (on the order of a few eVs [47]), and R is close to 1. Given that both the parent and daughter ions share the same A/q value and their relative mass difference $\Delta M/M < 10^{-4}$, the mass-dependent error becomes insignificant compared to the statistical uncertainty achieved in the measurements. Additionally, the contribution of uncertainty to the Q value arising from the mass uncertainty of the daughter ion chosen as a reference, 0.16 keV/ c^2 for ^{97}Mo [34], can be safely disregarded.

TABLE I. Final results from the analysis of the mean cyclotron frequency ratio between the ground state of daughter ^{97}Mo and parent (^{97}Tc , $9/2^+$) nuclei. Frequency ratio \bar{R} , Q_{EC} values (in keV) and the mass excess (in keV/ c^2) of parent nuclei determined in this work are listed in comparison with the AME2020 values [34].

	\bar{R}	Q_{EC}	mass excess
^{97}Tc (AME2020)		320.0(40)	-87224.0(40)
^{97}Tc (This Work)	1.00 000 359 84(23)	324.82(21)	-87219.88(26)

III. RESULTS AND DISCUSSION

From the measurements of the cyclotron frequency ratio R , Q_{EC} was calculated via Eq. 3. As shown in Fig. 3, 20 PI-ICR measurement data sets were collected for $^{97}\text{Tc}^+ - ^{97}\text{Mo}^+$. In less than 5 minutes, a full scanning measurement (one cycle) of the magnetron phase, reduced cyclotron phase and center spot in sequence was completed for each ion species

TABLE II. Potential candidate transitions from the initial state (ground state) of the parent nucleus ^{97}Tc ($9/2^+$) to the final states in the daughter nucleus ^{97}Mo . The first column lists the excited final state of ^{97}Mo for the low Q value transition. The decay type is provided in the second column. The third to sixth columns present the derived decay Q_{EC} values, sourced from literature (Lit.) [34] and this work (T. W.), respectively. The seventh column displays the experimental excitation energy E^* [33]. The eighth column shows the confidence level (σ) of the Q_{EC}^* being positive. Columns nine to eleven, denoted as Δx , represent the distance of Q_{EC} values to the binding energy ϵ_x of the electrons in the daughter atoms, sourced from [48]. Spin-parity assignments and energy values enclosed in braces $\{\}$ signify uncertain assignments or uncertainties in excitation energy, resulting in uncertainties in the decay type or decay energy. All decay-energy and energy-level values are in units of keV.

Final state	Decay type	$Q_{\text{gs-gs}}$ (Lit.)	$Q_{\text{gs-gs}}$ (T. W.)	Q_{EC}^* (Lit.)	Q_{EC}^* (T. W.)	E^*	$Q/\delta Q$ (T. W.)	Δ_{L1} (T. W.)	Δ_{L2} (T. W.)	Δ_{M1} (T. W.)
^{97}Mo ($\{9/2^+\}$)	{allowed}	320.0(40)	324.82(21)	0.0(41)	4.8(10)	320.0(10)	4.8	2.0(10)	2.2(10)	4.3(10)
^{97}Mo ($5/2^+$, ground state)		320.0(40)	324.82(21)							

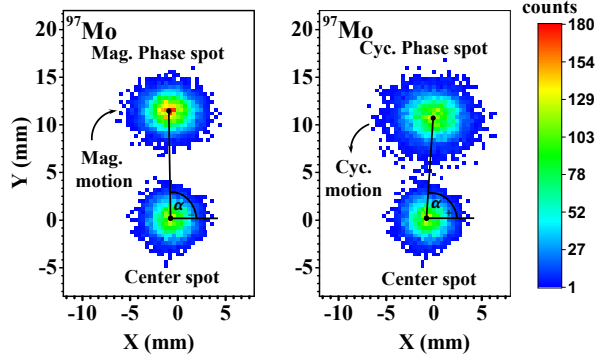


FIG. 2. (Color online). Example $^{97}\text{Mo}^+$ ion spots of center, reduced cyclotron (Cyc.) phase and magnetron (Mag.) phase on the 2-dimensional position-sensitive MCP detector after a typical PI-ICR excitation pattern with an accumulation time of 436 ms. The Mag. phase spot is demonstrated on the left side and the Cyc. phase spot on the right. The angle difference between these two spots in relation to the center is employed to calculate the cyclotron frequency ν_c . The color in each pixel corresponds to the number of ions as illustrated by color bars.

of the decay pair $^{97}\text{Tc}^+ - ^{97}\text{Mo}^+$. In the analysis, we determined the position of each spot using the maximum likelihood method. After summing a few cycles to obtain reasonable counts for fitting, phase angles were calculated based on the determined positions of the phase spots as demonstrated in Fig. 2. These phase angles allowed us to deduce the cyclotron frequencies of each ion species. By linearly interpolating the ν_c of the daughter ion $^{97}\text{Mo}^+$ (reference) to the time of the measurement of the parent ion $^{97}\text{Tc}^+$ (ion of interest), the cyclotron frequency ratio R was derived. To minimize potential cyclotron frequency shifts resulting from ion-ion interactions [49, 50], a median ion rate was constrained to 1-2 ions per bunch during the measurements. Bunches with fewer than five detected ions per bunch were considered during the data analysis. In the analysis, the count-rate related frequency shifts were not observed. The temporal fluctuation of the magnetic field $\delta_B(\nu_c)/\nu_c = \Delta t \times 2.01 \times 10^{-12}/\text{min}$ [43] is taken in account in the final results. Here, Δt represents the time interval between consecutive reference measurements. The contribution of magnetic field fluctuations to the final frequency ratio uncertainty was less than 10^{-10} , as the parent-

daughter measurements were interleaved with intervals less than 10 minutes. Additionally, the frequency shifts in the PI-ICR measurement caused by ion image distortions were ignored, as they were well below the statistical uncertainty. Furthermore, the fact that decay pair ions $^{97}\text{Tc}^+ - ^{97}\text{Mo}^+$ are mass doublets, cancels out many systematic uncertainties in the cyclotron frequency ratio. The weighted mean ratio \bar{R} of all single frequency ratios was calculated, considering the inner and outer errors to deduce the Birge ratio [51]. The maximum of the inner and outer errors served as the weight for computing \bar{R} . Results of our analysis including all data sets, in comparison to literature values, are presented in Fig. 3 and Table I. The final daughter-to-parent frequency ratio \bar{R} with its uncertainty is determined to be 1.000 003 598 4(23), resulting in a gs-to-gs Q value of 324.82(21) keV.

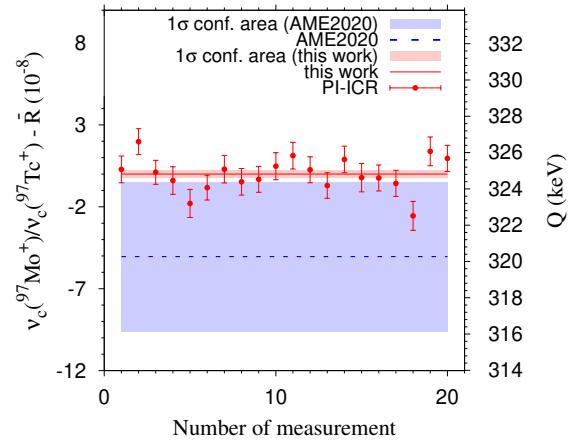


FIG. 3. (Color online). The measured experimental results from this work compared to the literature values [34, 52]. The deviations of the individually measured cyclotron frequency ratios R ($\nu_c(^{97}\text{Mo}^+)/\nu_c(^{97}\text{Tc}^+)$) from the measured value \bar{R} (left axis) and Q value (right axis) in this work are compared to values adopted from AME2020. The red points with uncertainties represent individual measurements using the PI-ICR method. Vertical brown dashed lines separate measurements conducted at different time slots. The weighted average value \bar{R} (referenced in Table I) is depicted by the solid red line, and its 1σ uncertainty band is shaded in red. The dashed blue line illustrates the difference between our new value and the one referenced in AME2020, with its 1σ uncertainty area shaded in blue.

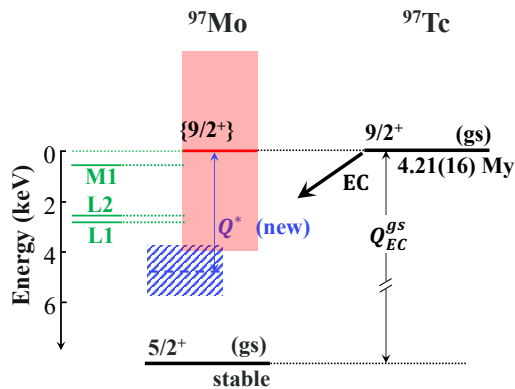


FIG. 4. (Color online). Partial EC scheme of ^{97}Tc decaying to $5/2^+$ ground and $\{9/2^+\}$ final states, the spin-parity assignment being uncertain for the latter state. The dashed green horizontal lines extending from the left indicate the threshold energy for the marked electron orbitals from which the EC can happen. The boxes with a red horizontal line show the Q_{EC} value using data from literature [34, 52] with 1σ uncertainty in comparison to the Q value from this work (hatched blue box). Our results indicate that EC to the $\{9/2^+\}$ state can occur only from the L1 orbital or higher, while the data from literature cannot give a conclusive clue of whether there are any allowed electron orbitals higher than the K orbital for EC to occur.

The gs-to-gs Q_{EC} value of 324.82(21) keV obtained from this work, which represents the first direct measurement, is approximately 19 times more precise than the value deduced from the evaluated masses in AME2020 [34, 52]. The measured Q_{EC} value has a deviation of 4.8(40) keV from the AME2020 value and is $\approx 1\sigma$ larger.

In the case of EC, the closer is the Q value of the decay to one of the ionization energies of the captured electrons, the larger the resonance enhancement of the rate near the endpoint, where the effects of a non-vanishing neutrino mass are relevant. Which orbital electrons take part in the EC process and the absolute Q values of the decays are crucial for modelling the spectrum shape near the endpoint. The current precision deduced from literature [33, 34, 52] does not allow a definitive conclusion on whether any other electron orbitals allow EC to occur for the transition $^{97}\text{Tc} (9/2^+) \rightarrow ^{97}\text{Mo}^* (320.0 \text{ keV})$. In this work, the high-precision Q -value measurement allows an unambiguous characterization of all the possible lines in the EC spectrum at a significance level of at least 2σ for the transition. This makes the modeling of its shape possible. The high-precision EC energy measured from this work, together with the nuclear energy level data from Ref. [33] of the excited state of ^{97}Mo as tabulated in Table II, was used to determine the gs-to-es Q value (Q_{EC}^*) of the candidate state. The newly determined Q_{EC}^* confirms that the decay of the ground state of ^{97}Tc to the excited state of interest is energetically allowed with a confidence level of more than 4σ , as shown in Table II. A comparison of the Q values of the gs-to-es EC transition from this work to the value derived from AME2020 is shown in Fig. 4. As tabulated in Table II, Δ_x gives the distance of the Q_{EC}^* value to the binding energy ε_x [48] of the electrons in the allowed daughter atomic shells ($x = \text{L1, L2, and other electrons from s levels and } p_{1/2} \text{ levels}$

from the third and higher shells). For the state with the excitation energy of 320.0(10) keV, the captures of electrons occupying the L1 and higher shells for the transition $^{97}\text{Tc} (9/2^+) \rightarrow ^{97}\text{Mo}^*$ are energetically allowed as indicated in Fig. 4. The transition $^{97}\text{Tc} (9/2^+) \rightarrow ^{97}\text{Mo}^* (320.0 \text{ keV})$, giving the values of 2.0(10) keV and 2.2(10) keV for the distance of Q_{EC}^* to the allowed binding energies $\varepsilon_{\text{L1}} = 2.866 \text{ keV}$ and $\varepsilon_{\text{L2}} = 2.625 \text{ keV}$ [48], is potentially of the allowed Fermi plus Gamow-Teller type. This transition is of high interest for future neutrino mass determination due to a possible high branching ratio. To confirm whether the emitted neutrino energy 2.0(10) keV is ultra-low, further high-precision measurements of the excitation energy of the state are required. Moreover, the parity of this state needs to be determined to verify the decay type of the transition to this state.

IV. THEORETICAL PREDICTIONS

Two calculation methods are employed to predict the distribution of energy released in the decay, the transition half-life and their error spread, namely the atomic many-electron Dirac–Hartree–Fock–Slater (DHFS) self-consistent method and the Nuclear Shell Model (NSM) many-nucleon framework. For the atomic-structure calculations we made use of the RADIAL subroutine package [53], which also contains the DHFS.F code, while for the NSM we employed the NuShellX@MSU code [54].

In our calculation we consider the initial atom in its ground state. The electronic structure of the final atom is constructed starting from the configuration of the initial atom with an electron hole in the shell from where it was captured. When the nucleus captures the electron, the other electrons (the spectator electrons) undergo processes that impact the decay rate. A couple of important corrections related to these processes are considered [32]: exchange and overlap corrections, shake-up and shake-off effects.

The atomic shells are denoted using the main quantum number n , and the relativistic quantum number κ as $x = (n, \kappa)$. In order to compute the released energy distribution of an allowed EC event we sum all the contributions from the atomic shells with the relativistic quantum number $\kappa = \pm 1$ as:

$$\rho(E') = \frac{G_\beta^2}{(2\pi)^2} C \sum_x n_x \beta_x^2 B_x S_x p_\nu E_\nu \frac{\Gamma_x / (2\pi)}{(E' - \varepsilon_x)^2 + \Gamma_x^2 / 4}. \quad (4)$$

Here we employ two corrections, namely the exchange and overlap correction represented by the B_x factor and the shake-up and shake-off corrections introduced as the S_x factor [55]. The Coulomb amplitude is calculated for the initial atom and is represented by β_x . The Cabibbo angle θ_C and the Fermi constant G_F are present in $G_\beta = G_F \cos \theta_C$. The relative occupancy of the shell is denoted as n_x . The energy and momentum of the emitted neutrino are represented as E_ν and $p_\nu = \sqrt{E_\nu^2 - m_\nu^2}$, with m_ν being the neutrino mass. A recent improvement [56] in the computation of the relaxation energy following the capture is the usage of total binding energy as $\varepsilon_x = |T_{\text{g.s.}}| - |T_x|$, where $T_{\text{g.s.}}$ indicates the energy of the final

TABLE III. Computed half-lives for the EC decay of ^{97}Tc to the excited state (320.0 keV) in ^{97}Mo , with the Q_{EC}^* value shown in Table II. The errors are computed according to the approach presented in Sec. IV A.

Channel	Interaction	Total half-life (10^4yr)	L1 (10^4yr)	L2 (10^7yr)	M1 (10^4yr)	M2 (10^6yr)	N1 (10^5yr)	N2 (10^7yr)	O1 (10^6yr)
L1 allowed	jj45pnb	$19^{+17}_{-0.7}$	46^{+120}_{-26}	$2.2^{+5.0}_{-1.2}$	47^{+32}_{-17}	26^{+18}_{-10}	20^{+12}_{-7}	13^{+8}_{-4}	42^{+25}_{-15}
L1 allowed	glekpn	$2.1^{+1.8}_{-0.7}$	$5.0^{+14}_{-2.9}$	$0.25^{+0.50}_{-0.13}$	$5.2^{+4.0}_{-1.9}$	$2.9^{+2.0}_{-1.1}$	$2.2^{+1.3}_{-0.8}$	$1.4^{+0.9}_{-0.5}$	$4.7^{+2.8}_{-1.6}$
L1 forbidden	jj45pnb	93^{+7}_{-6}	—	570^{+4000}_{-340}	169^{+50}_{-34}	91^{+27}_{-18}	60^{+18}_{-12}	38^{+11}_{-8}	127^{+40}_{-25}
L1 forbidden	glekpn	$10^{+0.8}_{-0.6}$	—	60^{+500}_{-40}	$19^{+5.0}_{-4.0}$	$10^{+3.0}_{-2.1}$	$6.7^{+1.9}_{-1.4}$	$4.3^{+1.2}_{-0.9}$	$14^{+4}_{-2.9}$

atom in its ground state, while x represents the energy of the excited state of the final atom with a hole in the x shell. The Γ_x represents the intrinsic line-widths of Breit-Wigner resonances centered at ε_x and they were taken from [57]. The nuclear structure part is represented by the C factor as:

$$C = \frac{1}{2J_i + 1} (g_V^2 |M_F|^2 + g_A^2 |M_{GT}|^2), \quad (5)$$

with g_V being the weak vector coupling, and g_A and J_i being the weak axial coupling and the angular momentum of the initial nucleus. The Fermi nuclear matrix element is denoted by M_F and the Gamow-Teller nuclear matrix element is denoted as M_{GT} .

To compute the decay probability $\lambda(E)$ in the interval $(0, E)$ we integrated the distribution of the released energy:

$$\lambda(E) = \int_0^E \rho(E') dE', \quad (6)$$

The energy E variable respects the relation $E = Q_{\text{EC}}^* - E_v$. By using the narrow-width approximation, the total decay rate can be written as $\lambda = \sum_x \lambda_x$, with the partial decay constant defined as:

$$\lambda_x = \frac{G_\beta^2}{(2\pi)^2} C n_x \beta_x^2 B_x S_x p_{vx} (Q_{\text{EC}}^* - \varepsilon_x), \quad (7)$$

where $p_{vx} = \sqrt{(Q_{\text{EC}}^* - \varepsilon_x)^2 - m_v^2}$.

In Table III, we present the predicted half-lives and associated uncertainties for the decay of ^{97}Tc to the excited state of ^{97}Mo , corresponding to the experimental energy $E^* = 320.0$ keV, across all relevant atomic shells. In the top two lines, we consider the L1 channel to be energetically possible (L1 allowed), while in the bottom two lines, we assume that the capture of L1 electrons is not energetically possible, but the capture from L2 is possible (L1 forbidden). As can be seen, there is a significant difference between the upper and lower error because the Q -value spans a considerable interval of values, and it appears in quadratic form in the half-life time formula.

In Fig. 5 we present the normalized distributions of released energy within a shaded-in-blue 68% confidence band between the blue curves. Considering a Gaussian distribution for the Q -value 97.3% of cases permit the capture of an electron from the L1 shell (bottom plot). In 1.2% the L1 channel is

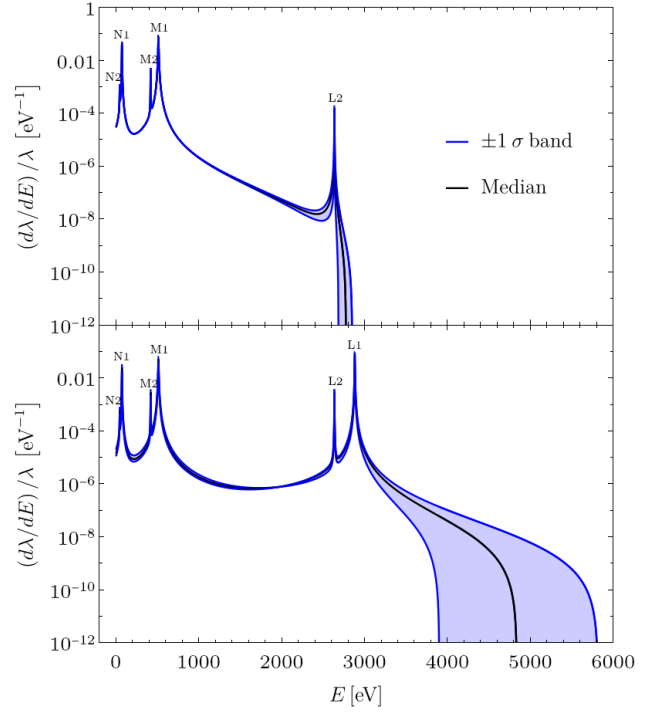


FIG. 5. Normalized distributions of released energy as a function of E in the statistical approach, Sec. IV A. We represented the 68% confidence interval shaded in blue with a dark blue contour. The blue lines indicate the 1σ distributions. The black line represents the median value of the normalized energy distribution at each energy point. The plots are for EC decay of ^{97}Tc to the excited state of interest in ^{97}Mo with a $Q_{\text{EC}}^* = 4.8(10)$ keV. The Q value follows a broad Gaussian distribution. For 97.3% of the elements in the distribution, the L1 channel is energetically possible (bottom plot). For 1.2% of them, the L1 channel is energetically forbidden, but the L2 channel is possible (top plot).

energetically impossible but the capture from the L2 sub-shell is possible (top plot). The other 1.5% of cases were not presented here, due to their decreasing probability of occurrence. The black line represents the median values for each energy point in the graph. The interval was obtained as described in section IV A. This analysis shows the high dependence of the normalized distribution on the Q_{EC}^* value, especially in the interesting region at the end of the spectrum. The biggest impact in the error of Q_{EC}^* comes from the uncertainty in the energy of the level of interest in the final nucleus. Thus a better as-

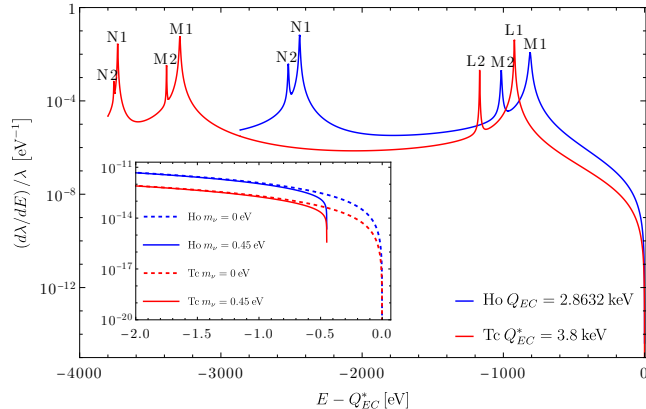


FIG. 6. Normalized distributions of released energy in the EC decay of ^{97}Tc in the transitions to the excited state of ^{97}Mo , of interest here, as functions of $E - Q_{\text{EC}}^*$. The blue line corresponds to the decay to the excited final state of energy $E^* = 320.0$ keV and with $Q_{\text{EC}}^* = 3.8$ keV, which is 1σ away from the central value of $Q_{\text{EC}}^* = 4.8$ keV. L1, L2, M1, and N1 indicate subshells from which the electron was captured. The M2, N2 and O1 subshells are harder to distinguish and are not labeled.

assessment of the energy of this level is necessary in order to have a more well-defined distribution of energy at Q_{EC}^* .

The current measurement of the Q_{EC}^* value with the associated error does not give a definite picture of the capture process. In order to investigate the implications of the associated uncertainties, we present in Fig. 6 a comparison between the normalized distribution of released energy as a function of the energy, $E - Q_{\text{EC}}^*$, for the decay of ^{97}Tc to excited state of ^{97}Mo with $Q_{\text{EC}}^* = 3.8$ keV, within 1σ range of the experimental central value, and ^{163}Ho to the ground state of ^{163}Dy with $Q_{\text{EC}} = 2.8623$ keV. As can be seen in the enlarged scale in the inset of Fig. 6, the neutrino-mass-sensitive region provides a higher EC event rate for ^{97}Tc for this Q value, making it comparable with the rate for ^{163}Ho . Also, this inset shows exactly the impact of the neutrino mass on the shape of the spectrum and how it could be highlighted. The long half-life of about 4 My for ^{97}Tc renders it a good candidate for future long-term neutrino-mass measurements.

A. Statistical approach

In order to calculate the propagation of errors in the half-life and the 68% band in the normalized distributions of released energy as shown in Fig. 5, we employed the pseudo-experiment technique. This method involves the sampling of parameters that potentially fluctuate from probability distribution functions (PDFs). For each set of parameters the half-life times and the normalized distribution of released energy are computed, thus obtaining their PDFs. The central values are obtained as medians of the PDFs. For the two-sided bounds we took the element at 0.16 and 0.84 of the CPDFs. The uncertainties are reported as the difference between each bound

and the median value.

We took into account Q_{EC}^* and g_A as sources of uncertainty. Assuming a Gaussian distribution of Q_{EC}^* , in about 2.7% cases the capture from the L1 sub-shell will not be energetically possible. Thus, we split the sampled values into groups and considered two in the current study. For the first group, the capture of the L1 electron is possible (L1 allowed), while for the second, the L1 channel is energetically forbidden, and the L2 channel is energetically possible (L1 forbidden). For each group we plotted the median and the 1σ band of the normalized distribution of released energy. For the distribution of g_A we have used a uniform distribution with values between 0.7 and 1.0. We consider a number of 10^6 pseudo-experiments. In particular, for the normalized distributions of released energy, we constructed a uniform grid of 10^4 points for E . In each point the procedure described above was applied.

V. CONCLUSION AND OUTLOOK

A direct high-precision gs-to-gs EC-decay Q -value measurement of $^{97}\text{Tc} (9/2^+) \rightarrow ^{97}\text{Mo} (5/2^+)$ was performed using the PI-ICR technique at the JYFLTRAP Penning-trap mass spectrometer. A Q value of 324.82(21) keV was obtained and the precision was improved by a factor of around 19 compared to literature. The measurement also improved the mass excess of ^{97}Tc , $-87219.88(26)$ keV/ c^2 , by a factor of 15 compared to the previously measured value. With the refined gs-to-gs Q value, the candidate transition of $^{97}\text{Tc} (9/2^+) \rightarrow ^{97}\text{Mo}^* (320.0$ keV) was validated to be energetically allowed. This also allows an unambiguous characterization of all the possible lines in the EC spectrum of this transition at a significance level of at least 2σ . The transition to the 320.0-keV state with a possible allowed decay type, has a small distance of 2.0(1.0) keV for the gs-to-es Q_{EC}^* to the binding energy of the electrons in the allowed daughter atomic shell L1. For further confirmation of whether this lowest emitted neutrino energy is ultra-low, the excitation energy needs to be determined with higher precision and accuracy. The atomic self-consistent many-electron Dirac-Hartree-Fock-Slater method and the nuclear shell model were utilized to predict the partial decay half-lives and energy distributions of gs-to-es EC transitions in ^{97}Tc with low Q values. To calculate error propagation in half-life and the 68% confidence interval for normalized energy distributions, a pseudo-experiment technique was introduced. Multiple corrections, such as exchange, overlap, shake-up, and shake-off effects, were accounted for in these predictions for modelling the spectrum shape near the endpoint.

ACKNOWLEDGMENTS

We acknowledge the staff of the Accelerator Laboratory of University of Jyväskylä (JYFL-ACCLAB) for providing stable online beam. We thank the support by the Academy of Finland with projects No. 306980, 312544, 275389, 284516, 295207, 314733, 315179, 327629, 320062, 354589,

345869 and 354968. The support by the EU Horizon 2020 research and innovation program under grant No. 771036 (ERC CoG MAIDEN) is acknowledged. This project has received funding from the European Union's Horizon 2020 research and innovation programme under grant agreement No. 861198-LISA-H2020-MSCA-ITN-2019. V.A.S., O.N., S.S.,

J.S., and J.K. acknowledge support from the NEPTUN project (PNRR-I8/C9-CF264, Contract No. 760100/23.05.2023 of the Romanian Ministry of Research, Innovation and Digitization). The work leading to this publication was supported by the Deutsche Forschungsgemeinschaft (DFG, German Research Foundation) - AY 155/2-1.

-
- [1] S. T. Petcov, *Adv. High Energy Phys.* **2013**, 1 (2013).
- [2] J. Lesgourgues and S. Pastor, *Physics Reports* **429**, 307 (2006).
- [3] Y. Fukuda, T. Hayakawa, E. Ichihara, K. Inoue, K. Ishihara, H. Ishino, Y. Itow, T. Kajita, J. Kameda, S. Kasuga, K. Kobayashi, Y. Kobayashi, Y. Koshio, M. Miura, M. Nakahata, S. Nakayama, A. Okada, K. Okumura, N. Sakurai, M. Shiozawa, Y. Suzuki, Y. Takeuchi, Y. Totsuka, S. Yamada, M. Earl, A. Habig, E. Kearns, M. D. Messier, K. Scholberg, J. L. Stone, L. R. Sulak, C. W. Walter, M. Goldhaber, T. Barszczak, D. Casper, W. Gajewski, P. G. Halverson, J. Hsu, W. R. Kropp, L. R. Price, F. Reines, M. Smy, H. W. Sobel, M. R. Vagins, K. S. Ganezer, W. E. Keig, R. W. Ellsworth, S. Tasaka, J. W. Flanagan, A. Kibayashi, J. G. Learned, S. Matsuno, V. J. Stenger, D. Takemori, T. Ishii, J. Kanzaki, T. Kobayashi, S. Mine, K. Nakamura, K. Nishikawa, Y. Oyama, A. Sakai, M. Sakuda, O. Sasaki, S. Echigo, M. Kohama, A. T. Suzuki, T. J. Haines, E. Blaufuss, B. K. Kim, R. Sanford, R. Svoboda, M. L. Chen, Z. Conner, J. A. Goodman, G. W. Sullivan, J. Hill, C. K. Jung, K. Martens, C. Mauger, C. Mc Grew, E. Sharkey, B. Viren, C. Yanagisawa, W. Doki, K. Miyano, H. Okazawa, C. Saji, M. Takahata, Y. Nagashima, M. Takita, T. Yamaguchi, M. Yoshida, S. B. Kim, M. Etoh, K. Fujita, A. Hasegawa, T. Hasegawa, S. Hatakeyama, T. Iwamoto, M. Koga, T. Maruyama, H. Ogawa, J. Shirai, A. Suzuki, F. Tsushima, M. Koshihara, M. Nemoto, K. Nishijima, T. Futagami, Y. Hayato, Y. Kanaya, K. Kaneyuki, Y. Watanabe, D. Kielczewska, R. A. Doyle, J. S. George, A. L. Stachyra, L. L. Wai, R. J. Wilkes, and K. K. Young, *Physical Review Letters* **81**, 1562 (1998), arXiv:9807003 [hep-ex].
- [4] SNO Collaboration, *Physical Review Letters* **89**, 1 (2002), arXiv:0204008 [nucl-ex].
- [5] M. Gerbino and M. Lattanzi, *Frontiers in Physics* **5** (2018), 10.3389/fphy.2017.00070.
- [6] G. Drexlin, V. Hannen, S. Mertens, and C. Weinheimer, *Advances in High Energy Physics* **2013**, 1 (2013), arXiv:1307.0101.
- [7] M. Aker, K. Altenmüller, M. Arenz, M. Babutzka, J. Barrett, S. Bauer, M. Beck, A. Beglarian, J. Behrens, T. Bergmann, U. Besserer, K. Blaum, F. Block, S. Bobien, K. Bokeloh, J. Bonn, B. Bornschein, L. Bornschein, H. Bouquet, T. Brunst, T. S. Caldwell, L. La Cascio, S. Chilingaryan, W. Choi, T. J. Corona, K. Debowski, M. Deffert, M. Descher, P. J. Doe, O. Dragoun, G. Drexlin, J. A. Dunmore, S. Dyba, F. Edzards, L. Eisenblätter, K. Eitel, E. Ellinger, R. Engel, S. Enomoto, M. Erhard, D. Eversheim, M. Fedkevych, A. Felden, S. Fischer, B. Flatt, J. A. Formaggio, F. M. Fränkle, G. B. Franklin, H. Frankrone, F. Friedel, D. Fuchs, A. Fulst, D. Furse, K. Gauda, H. Gemmeke, W. Gil, F. Glück, S. Görhardt, S. Groh, S. Grohmann, R. Grössle, R. Gumbshaimer, M. Ha Minh, M. Hackenjos, V. Hannen, F. Harms, J. Hartmann, N. Haußmann, F. Heizmann, K. Helbing, S. Hickford, D. Hilk, B. Hillen, D. Hillesheimer, D. Hinz, T. Höhn, B. Holzapfel, S. Holzmann, T. Houdy, M. A. Howe, A. Huber, T. M. James, A. Jansen, A. Kaboth, C. Karl, O. Kazachenko, J. Kellerer, N. Kernert, L. Kippenbrock, M. Kleesiek, M. Klein, C. Köhler, L. Köllenberger, A. Kopmann, M. Korzeczek, A. Kosmider, A. Kovalík, B. Krasch, M. Krause, H. Krause, L. Kuckert, B. Kuffner, N. Kunka, T. Lasserre, T. L. Le, O. Lebeda, M. Leber, B. Lehnert, J. Letnev, F. Leven, S. Lichter, V. M. Lobashev, A. Lokhov, M. MacHatschek, E. Malcherek, K. Müller, M. Mark, A. Marsteller, E. L. Martin, C. Melzer, A. Menshikov, S. Mertens, L. I. Minter, S. Mirz, B. Monreal, P. I. Morales Guzmán, K. Müller, U. Naumann, W. Ndeke, H. Neumann, S. Niemes, M. Noe, N. S. Oblath, H. W. Ortjohann, A. Osipowicz, B. Ostrick, E. Otten, D. S. Parno, D. G. Phillips, P. Plischke, A. Pollithy, A. W. Poon, J. Pouryamout, M. Prall, F. Priester, M. Röllig, C. Röttele, P. C. Ranitzsch, O. Rest, R. Rinderspacher, R. G. Robertson, C. Rodenbeck, P. Rohr, C. Roll, S. Rupp, M. Ryšavý, R. Sack, A. Saenz, P. Schäfer, L. Schimpf, K. Schlösser, M. Schlösser, L. Schlüter, H. Schön, K. Schönung, M. Schrank, B. Schulz, J. Schwarz, H. Seitz-Moskaliuk, W. Seller, V. Sibille, D. Siegmann, A. Skasyrskaya, M. Slezák, A. Špalek, F. Spanier, M. Steidl, N. Steinbrink, M. Sturm, M. Suesser, M. Sun, D. Tcherniakhovski, H. H. Telle, T. Thümmeler, L. A. Thorne, N. Titov, I. Tkachev, N. Trost, K. Urban, D. Vénos, K. Valerius, B. A. Vandevender, R. Vianden, A. P. Vizcaya Hernández, B. L. Wall, S. Wüstling, M. Weber, C. Weinheimer, C. Weiss, S. Welte, J. Wendel, K. J. Wierman, J. F. Wilkerson, J. Wolf, W. Xu, Y. R. Yen, M. Zacher, S. Zadorozhny, M. Zbořil, and G. Zeller, *Physical Review Letters* **123**, 1 (2019), arXiv:1909.06048.
- [8] M. Aker, A. Beglarian, J. Behrens, A. Berlev, U. Besserer, B. Bieringer, F. Block, B. Bornschein, L. Bornschein, M. Böttcher, T. Brunst, T. S. Caldwell, R. M. D. Carney, L. L. Cascio, S. Chilingaryan, W. Choi, K. Debowski, M. Deffert, M. Descher, D. D. Barrero, P. J. Doe, O. Dragoun, G. Drexlin, K. Eitel, E. Ellinger, R. Engel, S. Enomoto, A. Felden, J. A. Formaggio, F. M. Fränkle, G. B. Franklin, F. Friedel, A. Fulst, K. Gauda, W. Gil, F. Glück, R. Grössle, R. Gumbshaimer, V. Gupta, T. Höhn, V. Hannen, N. Haußmann, K. Helbing, S. Hickford, R. Hiller, D. Hillesheimer, D. Hinz, T. Houdy, A. Huber, A. Jansen, C. Karl, F. Kellerer, J. Kellerer, M. Klein, C. Köhler, L. Köllenberger, A. Kopmann, M. Korzeczek, A. Kovalík, B. Krasch, H. Krause, N. Kunka, T. Lasserre, T. L. Le, O. Lebeda, B. Lehnert, A. Lokhov, M. Machatschek, E. Malcherek, M. Mark, A. Marsteller, E. L. Martin, C. Melzer, A. Menshikov, S. Mertens, J. Mostafa, K. Müller, S. Niemes, P. Oelmann, D. S. Parno, A. W. P. Poon, J. M. L. Poyato, F. Priester, M. Röllig, C. Röttele, R. G. H. Robertson, W. Rodejohann, C. Rodenbeck, M. Ryšavý, R. Sack, A. Saenz, P. Schäfer, A. Schaller, L. Schimpf, K. Schlösser, M. Schlösser, L. Schlüter, S. Schneidewind, M. Schrank, B. Schulz, A. Schwemmer, M. Šefčík, V. Sibille, D. Siegmann, M. Slezák, M. Steidl, M. Sturm, M. Sun, D. Tcherniakhovski, H. H. Telle, L. A. Thorne, T. Thümmeler, N. Titov,

- I. Tkachev, K. Urban, K. Valerius, D. Vénos, A. P. V. Hernández, C. Weinheimer, S. Welte, J. Wendel, J. F. Wilkerson, J. Wolf, S. Wüstling, W. Xu, Y. R. Yen, S. Zadorozhny, and G. Zeller, *Nature Physics* **18**, 160 (2022).
- [9] M. Aker, D. Batzler, A. Beglarian, J. Behrens, J. Beisenkötter, M. Biassoni, B. Bieringer, Y. Biondi, F. Block, S. Bobien, M. Böttcher, B. Bornschein, L. Bornschein, T. S. Caldwell, M. Carminati, A. Chatrabhuti, S. Chilingaryan, B. A. Daniel, K. Debowski, M. Descher, D. D. Barrero, P. J. Doe, O. Dragoun, G. Drexlin, F. Edzards, K. Eitel, E. Ellinger, R. Engel, S. Enomoto, A. Felden, C. Fengler, C. Fiorini, J. A. Formaggio, C. Forstner, F. M. Fränkle, K. Gauda, A. S. Gavin, W. Gil, F. Glück, S. Grohmann, R. Grössle, R. Gumbshaimer, N. Gutknecht, V. Hannen, L. Hasselmann, N. Haußmann, K. Helbing, H. Henke, S. Heyns, S. Hickford, R. Hiller, D. Hillesheimer, D. Hinz, T. Höhn, A. Huber, A. Jansen, C. Karl, J. Kellerer, K. Khosonthongkee, M. Kleifges, M. Klein, J. Kohpeiß, C. Köhler, L. Köllenberger, A. Kopmann, N. Kovač, A. Kovalík, H. Krause, L. L. Cascio, T. Lasserre, J. Lauer, T. Le, O. Lebeda, B. Lehnert, G. Li, A. Lokhov, M. Machatschek, M. Mark, A. Marsteller, E. L. Martin, C. Melzer, S. Mertens, S. Mohanty, J. Mostafa, K. Müller, A. Nava, H. Neumann, S. Niemes, A. Onillon, D. S. Parno, M. Pavan, U. Pinsook, A. W. P. Poon, J. M. L. Poyato, S. Pozzi, F. Priestler, J. Ráliš, S. Ramachandran, R. G. H. Robertson, C. Rodenbeck, M. Röllig, C. Röttele, M. Ryšavý, R. Sack, A. Saenz, R. Salomon, P. Schäfer, M. Schlösser, K. Schlösser, L. Schlüter, S. Schneidewind, U. Schnurr, M. Schrank, J. Schürmann, A. Schütz, A. Schwemmer, A. Schwenck, M. Šefčík, D. Siegmann, F. Simon, F. Spanier, D. Spreng, W. Sreethawong, M. Steidl, J. Štorek, X. Stribl, M. Sturm, N. Suwonjandee, N. T. Jerome, H. H. Telle, L. A. Thorne, T. Thümmler, S. Tirolf, N. Titov, I. Tkachev, K. Urban, K. Valerius, D. Vénos, C. Weinheimer, S. Welte, J. Wendel, C. Wiesinger, J. F. Wilkerson, J. Wolf, S. Wüstling, J. Wydra, W. Xu, S. Zadorozhny, and G. Zeller, “Direct neutrino-mass measurement based on 259 days of *katrin* data,” (2024), arXiv:2406.13516 [nucl-ex].
- [10] A. A. Esfahani, D. M. Asner, S. Böser, R. Cervantes, C. Claessens, L. de Viveiros, P. J. Doe, S. Doeleman, J. L. Fernandes, M. Fertl, E. C. Finn, J. A. Formaggio, D. Furse, M. Guigue, K. M. Heeger, A. M. Jones, K. Kazkaz, J. A. Kofron, C. Lamb, B. H. LaRoque, E. Machado, E. L. McBride, M. L. Miller, B. Monreal, P. Mohanmurthy, J. A. Nikkel, N. S. Oblath, W. C. Pettus, R. G. H. Robertson, L. J. Rosenberg, G. Rybka, D. Rysewyk, L. Saldaña, P. L. Slocum, M. G. Sternberg, J. R. Tedeschi, T. Thümmler, B. A. VanDevender, L. E. Vertatschitsch, M. Wachtendonk, J. Weintraub, N. L. Woods, A. Young, and E. M. Zayas, *Journal of Physics G: Nuclear and Particle Physics* **44**, 054004 (2017).
- [11] M. Betti, M. Biasotti, A. Boscá, F. Calle, N. Canci, G. Cavoto, C. Chang, A. Cocco, A. Colijn, J. Conrad, N. D’Ambrosio, N. D. Groot, P. de Salas, M. Favrezzani, A. Ferella, E. Ferri, P. García-Abia, I. García-Cortés, G. G. Gomez-Tejedor, S. Gariazzo, F. Gatti, C. Gentile, A. Giachero, J. Gudmundsson, Y. Hochberg, Y. Kahn, A. Kievsky, M. Lisanti, C. Mancini-Terracciano, G. Mangano, L. Marcucci, C. Mariani, J. Martínez, M. Messina, A. Molinero-Vela, E. Monticone, A. Moroño, A. Nucciotti, F. Pandolfi, S. Parlati, S. Pastor, J. Pedrós, C. P. de los Heros, O. Pisanti, A. Polosa, A. Puiui, I. Rago, Y. Raitses, M. Rajteri, N. Rossi, I. Rucandio, R. Santorelli, K. Schaeffner, C. Tully, M. Viviani, F. Zhao, and K. Zurek, *Journal of Cosmology and Astroparticle Physics* **2019**, 047 (2019).
- [12] L. Gastaldo, K. Blaum, A. Doerr, C. E. Düllmann, K. Eberhardt, S. Eliseev, C. Enss, A. Faessler, A. Fleischmann, S. Kempf, M. Krivoruchenko, S. Lahiri, M. Maiti, Y. N. Novikov, P. C. Ranitzsch, F. Simkovic, Z. Szusc, and M. Wegner, *Journal of Low Temperature Physics* **176**, 876 (2014), arXiv:1306.2655.
- [13] L. Gastaldo, K. Blaum, K. Chrysalidis, T. Day Goodacre, A. Domula, M. Door, H. Dorrer, C. E. Düllmann, K. Eberhardt, S. Eliseev, C. Enss, A. Faessler, P. Filianin, A. Fleischmann, D. Fonnesu, L. Gamer, R. Haas, C. Hassel, D. Hengstler, J. Jochum, K. Johnston, U. Kebschull, S. Kempf, T. Kieck, U. Köster, S. Lahiri, M. Maiti, F. Mantegazzini, B. Marsh, P. Neroutsos, Y. N. Novikov, P. C. Ranitzsch, S. Rothe, A. Rischka, A. Saenz, O. Sander, F. Schneider, S. Scholl, R. X. Schüssler, C. Schweiger, F. Simkovic, T. Stora, Z. Szücs, A. Türlér, M. Veinhard, M. Weber, M. Wegner, K. Wendt, and K. Zuber, *European Physical Journal: Special Topics* **226**, 1623 (2017).
- [14] C. Velte, F. Ahrens, A. Barth, K. Blaum, M. Braß, M. Door, H. Dorrer, C. E. Düllmann, S. Eliseev, C. Enss, P. Filianin, A. Fleischmann, L. Gastaldo, A. Goeggelmann, T. D. Goodacre, M. W. Haverkort, D. Hengstler, J. Jochum, K. Johnston, M. Keller, S. Kempf, T. Kieck, C. M. König, U. Köster, K. Kromer, F. Mantegazzini, B. Marsh, Y. N. Novikov, F. Piquemal, A. Riccio, D. Richter, A. Rischka, S. Rothe, R. X. Schüssler, C. Schweiger, T. Stora, M. Wegner, K. Wendt, M. Zampaolo, and K. Zuber, *The European Physical Journal C* **79** (2019), 10.1140/epjc/s10052-019-7513-x.
- [15] M. Haaranen and J. Suhonen, *The European Physical Journal A* **49**, 1 (2013).
- [16] J. Suhonen, *Physica Scripta* **89**, 54032 (2014).
- [17] H. Ejiri, J. Suhonen, and K. Zuber, *Physics Reports* **797**, 1 (2019).
- [18] R. Sandler, G. Bollen, N. D. Gamage, A. Hamaker, C. Izzo, D. Puentes, M. Redshaw, R. Ringle, and I. Yandow, *Physical Review C* **100**, 1 (2019), arXiv:1906.03335.
- [19] J. Kartheim, D. Atanasov, K. Blaum, S. Eliseev, P. Filianin, D. Lunney, V. Manea, M. Mougeot, D. Neidherr, Y. Novikov, L. Schweikhard, A. Welker, F. Wienholtz, and K. Zuber, *Hyperfine Interactions* **240**, 1 (2019), arXiv:1905.05510.
- [20] A. De Roubin, J. Kostensalo, T. Eronen, L. Canete, R. P. De Groot, A. Jokinen, A. Kankainen, D. A. Nesterenko, I. D. Moore, S. Rinta-Antila, J. Suhonen, and M. Vilén, *Physical Review Letters* **124**, 1 (2020), arXiv:2002.08282.
- [21] Z. Ge, T. Eronen, A. de Roubin, D. A. Nesterenko, M. Hukkanen, O. Beliuskina, R. de Groot, S. Geldhof, W. Gins, A. Kankainen, A. Koszorús, J. Kotila, J. Kostensalo, I. D. Moore, A. Raggio, S. Rinta-Antila, J. Suhonen, V. Virtanen, A. P. Weaver, A. Zadvornaya, and A. Jokinen, *Physical Review C* **103**, 065502 (2021).
- [22] Z. Ge, T. Eronen, K. S. Tyrin, J. Kotila, J. Kostensalo, D. A. Nesterenko, O. Beliuskina, R. de Groot, A. de Roubin, S. Geldhof, W. Gins, M. Hukkanen, A. Jokinen, A. Kankainen, A. Koszorús, M. I. Krivoruchenko, S. Kujanpää, I. D. Moore, A. Raggio, S. Rinta-Antila, J. Suhonen, V. Virtanen, A. P. Weaver, and A. Zadvornaya, *Phys. Rev. Lett.* **127**, 272301 (2021).
- [23] Z. Ge, T. Eronen, A. de Roubin, K. Tyrin, L. Canete, S. Geldhof, A. Jokinen, A. Kankainen, J. Kostensalo, J. Kotila, M. Krivoruchenko, I. Moore, D. Nesterenko, J. Suhonen, and M. Vilén, *Physics Letters B* **832**, 137226 (2022).
- [24] T. Eronen, Z. Ge, A. de Roubin, M. Ramalho, J. Kostensalo, J. Kotila, O. Beliuskina, C. Delafosse, S. Geldhof, W. Gins, M. Hukkanen, A. Jokinen, A. Kankainen, I. Moore, D. Nesterenko, M. Stryjczyk, and J. Suhonen, *Physics Letters*

- B 830**, 137135 (2022).
- [25] Z. Ge, T. Eronen, A. de Roubin, J. Kostensalo, J. Suhonen, D. A. Nesterenko, O. Beliuskina, R. de Groote, C. Delafosse, S. Geldhof, W. Gins, M. Hukkanen, A. Jokinen, A. Kankainen, J. Kotila, A. Koszorús, I. D. Moore, A. Raggio, S. Rinta-Antila, V. Virtanen, A. P. Weaver, and A. Zadornaya, *Phys. Rev. C* **106**, 015502 (2022).
- [26] M. Ramalho, Z. Ge, T. Eronen, D. A. Nesterenko, J. Jaatinen, A. Jokinen, A. Kankainen, J. Kostensalo, J. Kotila, M. I. Krivoruchenko, J. Suhonen, K. S. Tyrin, and V. Virtanen, *Phys. Rev. C* **106**, 015501 (2022).
- [27] N. D. Gamage, R. Sandler, F. Buchinger, J. A. Clark, D. Ray, R. Orford, W. S. Porter, M. Redshaw, G. Savard, K. S. Sharma, and A. A. Valverde, *Phys. Rev. C* **106**, 045503 (2022).
- [28] D. K. Kehlbeck, R. Bhandari, N. D. Gamage, M. Horana Gamage, K. G. Leach, X. Mougeot, and M. Redshaw, *Phys. Rev. C* **107**, 015504 (2023).
- [29] Z. Ge, T. Eronen, A. de Roubin, M. Ramalho, J. Kostensalo, J. Kotila, J. Suhonen, D. A. Nesterenko, A. Kankainen, P. Ascher, O. Beliuskina, M. Flayol, M. Gerbaux, S. Grévy, M. Hukkanen, A. Husson, A. Jaries, A. Jokinen, I. D. Moore, P. Pirinen, J. Romero, M. Stryczyk, V. Virtanen, and A. Zadornaya, *Phys. Rev. C* **108**, 045502 (2023).
- [30] A. Valverde, F. Kondev, B. Liu, D. Ray, M. Brodeur, D. Burdette, N. Callahan, A. Cannon, J. Clark, D. Hoff, R. Orford, W. Porter, G. Savard, K. Sharma, and L. Varriano, *Physics Letters B* **858**, 139037 (2024).
- [31] Z. Ge, T. Eronen, M. Ramalho, A. de Roubin, D. A. Nesterenko, A. Kankainen, O. Beliuskina, R. de Groote, S. Geldhof, W. Gins, M. Hukkanen, A. Jokinen, Á. Koszorús, J. Kotila, J. Kostensalo, I. D. Moore, P. Pirinen, A. Raggio, S. Rinta-Antila, V. A. Sevestrean, J. Suhonen, V. Virtanen, and A. Zadornaya, *Eur. Phys. J. A* **60** (2024), <https://doi.org/10.1140/epja/s10050-024-01317-3>.
- [32] Z. Ge, T. Eronen, V. A. Sevestrean, O. Nițescu, S. Stoica, M. Ramalho, J. Suhonen, A. de Roubin, D. Nesterenko, A. Kankainen, P. Ascher, S. Ayet San Andres, O. Beliuskina, P. Delahaye, M. Flayol, M. Gerbaux, S. Grévy, M. Hukkanen, A. Jaries, A. Jokinen, A. Husson, D. Kahl, J. Kostensalo, J. Kotila, I. Moore, S. Nikas, M. Stryczyk, and V. Virtanen, *Physics Letters B* **859**, 139094 (2024).
- [33] “National nuclear data center,” Available at <https://www.nndc.bnl.gov/> (2020/4/7) (2021).
- [34] M. Wang, W. Huang, F. Kondev, G. Audi, and S. Naimi, *Chinese Physics C* **45**, 030003 (2021).
- [35] I. D. Moore, T. Eronen, D. Gorelov, J. Hakala, A. Jokinen, A. Kankainen, V. S. Kolhinen, J. Koponen, H. Penttilä, I. Pohjalainen, M. Reponen, J. Rissanen, A. Saastamoinen, S. Rinta-Antila, V. Sonnenschein, and J. Äystö, *Nuclear Instruments and Methods in Physics Research, Section B: Beam Interactions with Materials and Atoms* **317**, 208 (2013).
- [36] V. S. Kolhinen, T. Eronen, D. Gorelov, J. Hakala, A. Jokinen, K. Jokiranta, A. Kankainen, M. Koikkalainen, J. Koponen, H. Kulmala, M. Lantz, A. Mattera, I. D. Moore, H. Penttilä, T. Pikkarainen, I. Pohjalainen, M. Reponen, S. Rinta-Antila, J. Rissanen, C. Rodríguez Triguero, K. Rytönen, A. Saastamoinen, A. Solders, V. Sonnenschein, and J. Äystö, *Nuclear Instruments and Methods in Physics Research, Section B: Beam Interactions with Materials and Atoms* **317**, 506 (2013).
- [37] P. Karvonen, I. D. Moore, T. Sonoda, T. Kessler, H. Penttilä, K. Peräjärvi, P. Ronkanen, and J. Äystö, *Nuclear Instruments and Methods in Physics Research, Section B: Beam Interactions with Materials and Atoms* **266**, 4794 (2008).
- [38] A. Nieminen, J. Huikari, A. Jokinen, J. Äystö, P. Campbell, and E. C. Cochrane, *Nuclear Instruments and Methods in Physics Research, Section A: Accelerators, Spectrometers, Detectors and Associated Equipment* **469**, 244 (2001).
- [39] M. Vilén, L. Canete, B. Cheal, A. Giatzoglou, R. de Groote, A. de Roubin, T. Eronen, S. Geldhof, A. Jokinen, A. Kankainen, I. D. Moore, D. A. Nesterenko, H. Penttilä, I. Pohjalainen, M. Reponen, and S. Rinta-Antila, *Nuclear Instruments and Methods in Physics Research, Section B: Beam Interactions with Materials and Atoms* **463**, 382 (2020).
- [40] T. Eronen, V. S. Kolhinen, V. V. Elomaa, D. Gorelov, U. Hager, J. Hakala, A. Jokinen, A. Kankainen, P. Karvonen, S. Kopecky, I. D. Moore, H. Penttilä, S. Rahaman, S. Rinta-Antila, J. Rissanen, A. Saastamoinen, J. Szerypo, C. Weber, and J. Äystö, *European Physical Journal A* **48**, 1 (2012).
- [41] G. Savard, S. Becker, G. Bollen, H. J. Kluge, R. B. Moore, T. Otto, L. Schweikhard, H. Stolzenberg, and U. Wiess, *Physics Letters A* **158**, 247 (1991).
- [42] T. Eronen, V.-V. Elomaa, U. Hager, J. Hakala, A. Jokinen, A. Kankainen, S. Rahaman, J. Rissanen, C. Weber, and J. Äystö, *Nuclear Instruments and Methods in Physics Research Section B: Beam Interactions with Materials and Atoms* **266**, 4527 (2008), proceedings of the XVth International Conference on Electromagnetic Isotope Separators and Techniques Related to their Applications.
- [43] D. A. Nesterenko, T. Eronen, Z. Ge, A. Kankainen, and M. Vilen, *Eur. Phys. J. A* **57**, 302 (2021).
- [44] D. A. Nesterenko, T. Eronen, A. Kankainen, L. Canete, A. Jokinen, I. D. Moore, H. Penttilä, S. Rinta-Antila, A. de Roubin, and M. Vilen, *European Physical Journal A* **54**, 0 (2018).
- [45] S. Eliseev, K. Blaum, M. Block, A. Dörr, C. Droese, T. Eronen, M. Goncharov, M. Höcker, J. Ketter, E. M. Ramirez, D. A. Nesterenko, Y. N. Novikov, and L. Schweikhard, *Applied Physics B: Lasers and Optics* **114**, 107 (2014).
- [46] S. Eliseev, K. Blaum, M. Block, C. Droese, M. Goncharov, E. Minaya Ramirez, D. A. Nesterenko, Y. N. Novikov, and L. Schweikhard, *Physical Review Letters* **110**, 82501 (2013).
- [47] A. Kramida, Yu. Ralchenko, J. Reader, and NIST ASD Team, NIST Atomic Spectra Database (ver. 5.8), [Online]. Available: <https://physics.nist.gov/asd> [2021, January 19]. National Institute of Standards and Technology, Gaithersburg, MD. (2020).
- [48] “X-ray data booklet,” Available at <https://xdb.lbl.gov> (2021/05/01) (2021).
- [49] A. Kellerbauer, K. Blaum, G. Bollen, F. Herfurth, H. J. Kluge, M. Kuckein, E. Sauvan, C. Scheidenberger, and L. Schweikhard, *European Physical Journal D* **22**, 53 (2003).
- [50] C. Roux, K. Blaum, M. Block, C. Droese, S. Eliseev, M. Goncharov, F. Herfurth, E. M. Ramirez, D. A. Nesterenko, Y. N. Novikov, and L. Schweikhard, *The European Physical Journal D* **67**, 1 (2013).
- [51] R. T. Birge, *Physical Review* **40**, 207 (1932).
- [52] W. Huang, M. Wang, F. Kondev, G. Audi, and S. Naimi, *Chinese Physics C* **45**, 030002 (2021).
- [53] F. Salvat and J. M. Fernández-Varea, *Computer Physics Communications* **240**, 165 (2019).
- [54] B. Brown and W. Rae, *Nuclear Data Sheets* **120**, 115 (2014).
- [55] X. Mougeot, *Applied Radiation and Isotopes* **134**, 225 (2018).
- [56] V. A. Sevestrean, O. Nițescu, S. Ghinescu, and S. Stoica, *Phys. Rev. A* **108**, 012810 (2023).
- [57] J. CAMPBELL and T. PAPP, *Atomic Data and Nuclear Data Tables* **77**, 1 (2001).